IEEE Photonics Journal
An IEEE Photonics Society Publication

Open Access

Robust Silicon Waveguide Polarization Rotator With an Amorphous Silicon Overlayer

Volume 6, Number 2, April 2014

Yule Xiong
Dan-Xia Xu
Jens H. Schmid
Pavel Cheben
Siegfried Janz
Winnie N. Ye

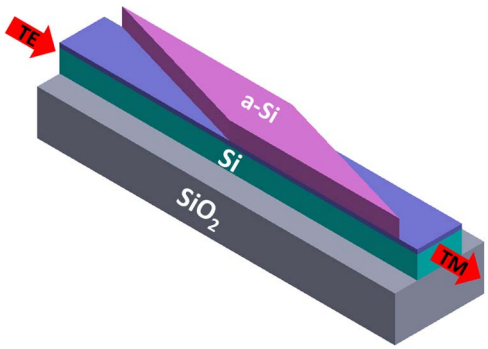

DOI: 10.1109/JPHOT.2014.2306827
1943-0655

IEEE photonics SOCIETY

IEEE

Robust Silicon Waveguide Polarization Rotator With an Amorphous Silicon Overlayer

Yule Xiong,[1,2] Dan-Xia Xu,[1] Jens H. Schmid,[1] Pavel Cheben,[1] Siegfried Janz,[1] and Winnie N. Ye[2]

[1]Information and Communications Technologies, National Research Council Canada, Ottawa, ON K1A 0R6, Canada
[2]Department of Electronics, Carleton University, Ottawa, ON K1S 5B6, Canada

DOI: 10.1109/JPHOT.2014.2306827

Manuscript received January 22, 2014; revised February 12, 2014; accepted February 13, 2014. Date of publication February 19, 2014; date of current version March 3, 2014. Corresponding author: Y. Xiong (e-mail: yule.xiong.ele@gmail.com).

Abstract: We propose a robust polarization rotator based on the mode-evolution mechanism. The polarization rotation in a silicon wire waveguide is achieved by forming an amorphous silicon (a-Si) overlayer and an SiO_2 spacer on top of the waveguide. A strip pattern of a constant width is designed to be etched through the overlayer at a specific angle with respect to the Si waveguide. The asymmetry in the a-Si overlayer affects the waveguide mode by rotating the modal axis. This polarization rotator design is amenable to comparatively simple fabrication compatible with standard silicon photonic processing for integration. The length of the rotation section is 17 μm, and the broadband operation is achieved with a rotation efficiency higher than 90% for a wavelength range exceeding 135 nm. A maximum polarization rotation efficiency of 99.5% is predicted by calculation.

Index Terms: Silicon waveguide, polarization rotation, amorphous silicon.

1. Introduction

Polarization management is an important research topic in the development of silicon photonic integrated circuits because of the high polarization sensitivity of silicon-wire waveguides [1]. To circumvent the intrinsic limitations imposed by waveguide polarization sensitivity, a polarization diversity approach is typically used in Si-wire photonic circuits [2]. In this approach, the input light of arbitrary polarization is first split into two orthogonal polarization states (quasi-TE and quasi-TM) by a polarization beam splitter, followed by rotating one of the polarization states by 90° using a polarization rotator. After independently processing these two signals of the identical polarization state, one of them is rotated back 90° using a second polarization rotator, and the two orthogonal components are recombined with a polarization beam splitter.

Two main polarization rotation mechanisms used in integrated optics are mode coupling [3], [4] and mode evolution [5]–[10]. Mode-coupling structures require phase matching and precisely tuned coupling. As such, mode-coupling structures (e.g. directional couplers) are inherently wavelength dependent and sensitive to fabrication variations [3], [4]. Mode-evolution structures, on the other hand, generally operates in a broad wavelength range and are more tolerant to dimensional changes [5]–[7]. Previously reported devices typically require precise lithographic alignments and high fabrication accuracy of small features. For example, in the mode evolution polarization splitter/rotator

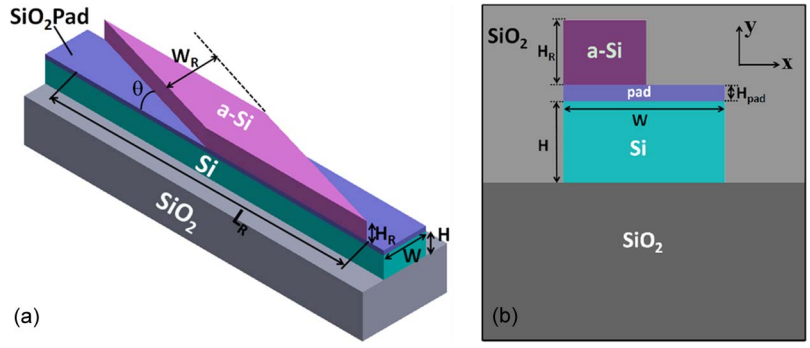

Fig. 1. (a) Schematic of the polarization rotator with a-Si overlayer. (b) Waveguide cross-section with asymmetric a-Si loading and SiO_2 upper cladding.

reported in [2], e-beam lithography was used to achieve the precise dimensional control of the asymmetric bi-level tapers with a minimum feature size of 70 nm. More recently, several groups have proposed and demonstrated mode evolution polarization rotators using asymmetric amorphous silicon (a-Si) overlayers [7], [8]. However, all these designs required geometrical modification for the access waveguide and precise placement of the a-Si overlayer relative to the access waveguide, which may reduce the manufacturing yield thus increasing the cost per individual device.

Here, we propose a novel polarization rotator design by simply loading a silicon wire waveguide with a diagonally positioned a-Si overlayer based on the mode evolution principle, as illustrated in Fig. 1. An a-Si layer is first deposited on a SOI wafer, separated by a thin etch-stop oxide layer. The single crystalline silicon (c-Si) wire waveguide is formed with the a-Si top layer. The a-Si layer is patterned with a strip of a constant width, tilted by an angle θ relative to the silicon access waveguide. The cross-section of the rotator is asymmetric with a varying a-Si width. This asymmetry induces polarization rotation. The cross-sectional structure of our design is similar to that reported in [6], [8]. Unlike in those designs, however, in our device the widths of the c-Si access waveguide and the a-Si overlayer both remain constant from a lithography point of view. Therefore high-precision lithographic alignment is not required. The varying cross-section geometry is introduced simply by placing the a-Si strip on top of the c-Si access waveguide at an angle. No loss penalty or changes in the rotation efficiency are observed in the fabrication tolerance range, as it is demonstrated in Section 3. Furthermore, unlike in mode coupling polarization rotators where air is typically used as superstrate to achieve vertical asymmetry, our design assumes SiO_2 upper cladding, allowing the polarization rotator to be readily integrated within a planar waveguide circuit.

2. Structure Design and Operation Principle

The proposed polarization rotator illustrated in Fig. 1 has a silicon access waveguide of width W and height H, separated from an a-Si overlayer by a thin SiO_2 pad layer of thickness H_{pad}. The a-Si layer is formed as a strip of thickness H_R and width W_R, positioned at a tilt angle θ with respect to the c-silicon waveguide. The length L_R of the polarization rotator is determined by θ and W_R. Although the polarization rotator described here can also function well with an air upper cladding, here we assume an SiO_2 upper cladding to facilitate integration with other components.

The performance of the polarization rotator is evaluated using the eigenmode expansion (EME) method and the three-dimensional finite-difference time-domain (3D-FDTD) simulations. We assume a quasi-TE input mode (E_x component dominant), but since the polarization rotator is reciprocal, equivalent results are obtained for a quasi-TM polarized input mode. In our simulations we assume the wavelength of 1550 nm, and the refractive indices of c-Si and a-Si of $n_{c-Si} = 3.476$ and $n_{a-Si} = 3.55$. The upper and lower SiO_2 cladding index is assumed $n_{SiO2} = 1.444$. The polarization rotator performance is examined for two heights of access wire waveguide: (i) H = 260 nm, which is similar to that reported for several mode evolution rotators [8], [9] and which has been extensively

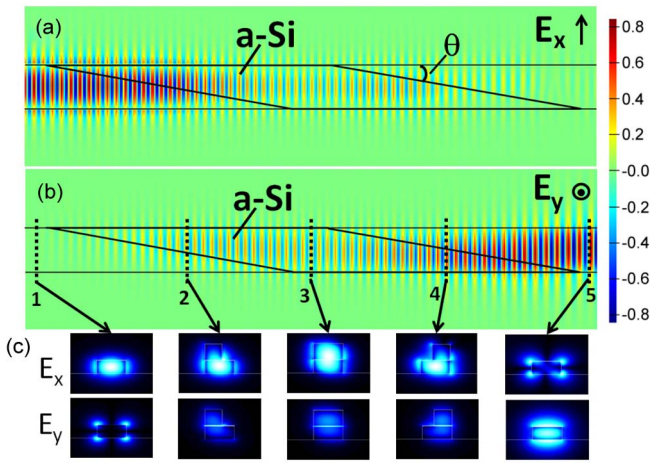

Fig. 2. Electric field components (a) E_x and (b) E_y evolution along the polarization rotator (top view), as calculated by a 3D-FDTD method. (c) Transverse electric field distributions at the corresponding positions along the polarization rotator.

used in evanescent filed biosensors operating in TM polarization [11], [12]; and (ii) H $=$ 220 nm, which is typically used in silicon photonics foundries with public access.

Fig. 2(a) and (b) shows the evolution of the electric field components E_x and E_y of the waveguide mode. Along the rotation section, the quasi-TE mode in the access waveguide is gradually coupled into the c-Si/a-Si composite waveguide where the mode becomes substantially hybridized as the a-Si width increases. The major component E_x of the input mode gradually transforms into the orthogonal E_y component and quasi-TE polarization is rotated to quasi-TM polarization at the rotator output, as shown in Fig. 2(c). Similarly, polarization rotation can be obtained from a quasi-TM input mode to quasi-TE output mode for the same device parameters, because of the reciprocity condition.

A thin SiO_2 pad layer is introduced in between the c-Si access waveguide and the a-Si overlayer to provide etch-stop for the a-Si layer. We choose a thin pad oxide layer of only 10 nm to frustrate slot waveguide effect [13]. This substantially improves the optical performance of the rotator, as it is further discussed in Section 3.

The polarization rotator performance is evaluated in terms of polarization rotation efficiency (PRE), which is the ratio of the power transferred between the two orthogonally polarized waveguide modes for a given input polarization state. For example, for the TE input, PRE is defined as the ratio of the output TM mode power to the input TE mode power: PRE $= P^{out}_{TM}/P^{in}_{TE}$. Other important device parameters include the insertion loss (IL), extinction ratio (ER), tolerance to dimensional variations and the operational wavelength range (bandwidth). In our design, we attempt to increase the access waveguide width W to reduce scattering loss due to sidewall roughness, and to minimize the rotator length L_R while maximizing the polarization rotation efficiency.

For a given access waveguide width W and a-Si height H_R, the PRE depends on the a-Si strip width W_R and tilt angle θ with respect to the access waveguide. Within a range of tilt angle θ, there exist a set of (θ, W_R) combinations that provide a high PRE, as shown in Fig. 3(a). For example, to meet PRE $> 99\%$, the tilt angle θ ranges are from 1.5° to 2.4° for $H_R = H = 220$ nm and W $= 390$ nm, and from 1.1° to 1.7° for $H_R = H = 260$ nm and W=430 nm. Although both θ and W_R determine the polarization rotator length, using a large θ is more effective in obtaining a small L_R. The design with the largest θ and PRE $> 99\%$ is chosen as the optimization goal. We also note that the rotation behavior is periodic with W_R, but this leads to a longer rotator section and the tolerance to the width inaccuracy of the access waveguide is correspondingly reduced.

Fig. 3(b) illustrates the total rotator length and the strip width W_R as a function of tilt angle θ for a scanning result similar to that presented in Fig. 3(a). To obtain a short rotator length (L_R), the largest angle, for which PRE is still more than 99%, is used. Therefore, the tilt angle θ is set to 2.4° for $H_R = H = 220$ nm, and 1.7° for $H_R = H = 260$ nm, as shown by the data points in Fig. 3(b).

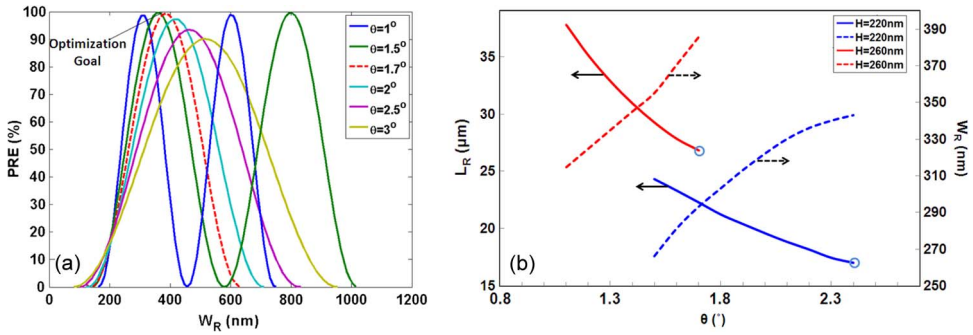

Fig. 3. (a) Polarization Rotation Efficiency (PRE) as a function of the a-Si strip width W_R for access waveguide width $W = 430$ nm; $H = H_R = 260$ nm. (b) Length of the rotation section L_R and the corresponding W_R as a function of tilt angle θ for two different heights H (220 nm and 260 nm) of the access waveguide; two heights (220 nm and 260 nm) of the access wire waveguide.

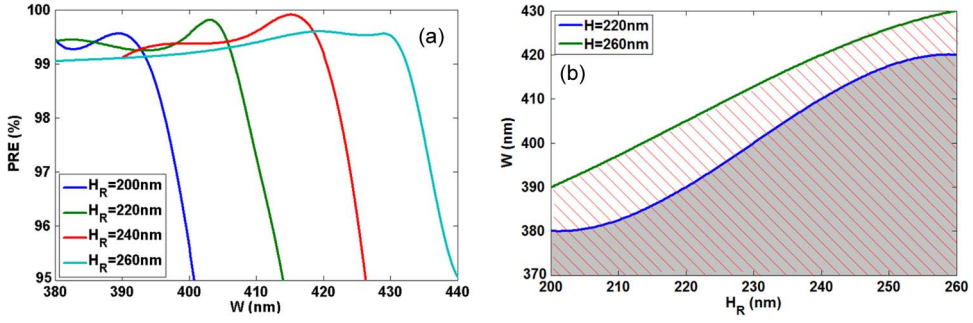

Fig. 4. (a) Polarization rotation efficiency as a function of the access waveguide width W for different thickness H_R of a-Si overlayer. (b) Possible combinations of the width of the access waveguide W and the height of the a-Si layer H_R for a PRE of > 99%. Grey area: $H = 220$ nm; hatched area: $H = 260$ nm.

As shown in Fig. 4(a), for a given a-Si thickness H_R, a range of W values can be used to obtain a high PRE [for optimized θ and W_R shown in Fig. 3(a)]. When the waveguide is too wide and the aspect ratio of the composite c-Si/a-Si waveguide is lower than 1.2, the rotation ceases to be efficient. The maximum width of the silicon core required to achieve PRE $> 99\%$ is shown in Fig. 4(b) as a function of a-Si overlayer height H_R, for 220 nm and 260 nm thick SOI. Given the same H_R, a smaller W is required for $H = 220$ nm, a trend which was also observed in a previous study [7]. However, a larger W can accommodate a larger H_R. In addition, a large W is preferred for reducing scattering loss, and for better dimensional tolerances, which will be discussed in detail in Section 3. From the fabrication point of view, a low aspect ratio in cross-section is desirable. Therefore, there is a trade-off between the maximum c-Si core width and the height of the a-Si overlayer. In the following, we choose the two layers to have the same thickness $(H = H_R)$ as a trade-off. The corresponding maximum widths of the silicon cores are $W = 390$ nm for $H = 220$ nm and $W = 430$ nm for $H = 260$ nm. The optimized designs have the following parameters (Table 1). On the other hand, for a TM input, the corresponding PREs are 98.4% for $H = 220$ nm, and 99.3% for $H = 260$ nm by using the parameters in Table 1. The polarization rotation performance of the rotator structures for the TM is expected to be similar to that of the TE.

3. Fabrication Tolerances

The designed asymmetric structures can be readily fabricated using the standard silicon photonics processing, and it is compatible with the processes for the high-efficiency surface grating couplers with an a-Si overlayer [14]. To investigate the robustness of our polarization rotator design, we calculate the polarization rotation efficiency as a function of several fabrication variations, shown in

TABLE 1

Optimized parameters of the rotator structures for H = 220 nm and H = 260 nm by assuming a TE input

W (nm)	H (nm)	W_R (nm)	H_R (nm)	θ (°)	L_R (μm)	PRE
390	220	343	220	2.4	17	99.0%
430	260	386	260	1.7	27	99.5%

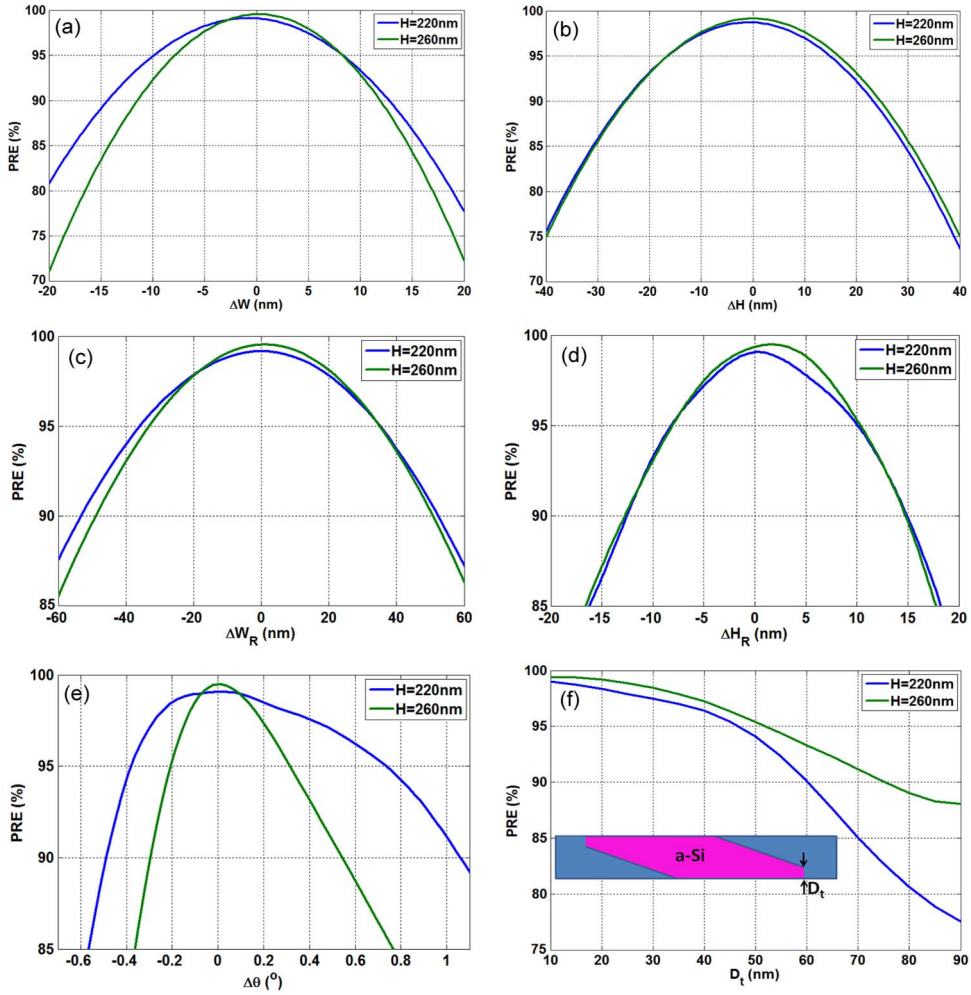

Fig. 5. Dependence of the polarization rotation efficiency (PRE) on structure geometrical tolerances calculated with fully vectorial EME simulations for: (a) Width of the access waveguide, ΔW; (b) height of the access waveguide, ΔH; (c) width of the a-Si patch, ΔW_R; (d) height of the a-Si patch, ΔH_R, (e) angle between the a-Si layer and the access waveguide, $\Delta\theta$; and (f) tip width of the a-Si layer, D_t. The optimal parameters are listed in Table 1; For H = 220 nm: H_R = 220 nm, W = 430 nm, W_R = 386 nm, and $\theta = 2.4°$; For H = 260 nm: H_R = 260 nm, W = 430 nm, W_R = 386 nm, and $\theta = 1.7°$.

Fig. 5 by assuming a TE input. For each scan of a given parameter, all other parameters remain constant at their nominal values. We determine the fabrication tolerances with a condition of PRE > 90%, with the results summarized in Table 2. In the following, the calculated fabrication tolerances refer to the condition of PRE > 90%.

It is observed from Fig. 5 and Table 2 that the PRE is most sensitive to the width of the silicon core (W), which is expected since W contributes significantly to the propagation constants of the

TABLE 2

Calculated tolerances of the polarization rotator structures for PRE > 90% and a TE input

H_{Si} (nm)	W (nm)	H (nm)	W_R (nm)	H_R (nm)	θ (°)	D_t (nm)
220	390±13	220±21	343±50	220±13	2.4±0.5	< 60
260	430±11	260±22	386±50	260±13	1.7±0.3	< 75

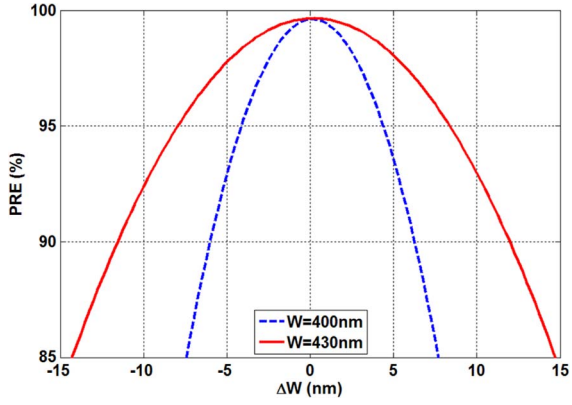

Fig. 6. Waveguide width tolerances for different widths of the access waveguide, calculated by fully vectorial EME simulations. Dash curve: W = 400 nm, H = H_R = 260 nm, W_R = 860 nm, $\theta = 3°$; Solid curve: W = 430 nm, H = H_R = 260 nm, W_R = 386 nm, $\theta = 1.7°$.

first two modes. As it is shown in Fig. 6, waveguides with smaller width W are more sensitive to the width variation, e.g. ΔW is only ±6 nm for W = 400 nm to meet the condition PRE > 90%. For this reason, larger waveguide widths are preferred. By using a waveguide of W = 430 nm, the width tolerance is improved to ±11 nm. For most lithography tools, angular alignment is highly accurate and an angle control of $< 0.3°$ is readily achievable. In practical consideration, the tip termination of the a-Si layer (D_t) has a finite width size. Fig. 5(f) shows calculated PRE efficiency as a function of D_t. Our starting simulation value for D_t is 10 nm, which is a reasonably achievable tip size using e-beam patterning. When $D_t < 60$ nm for H = 220 nm, and $D_t < 75$ nm for H = 260 nm, the PREs are > 90%. Finally, we found that a variation in the refractive index of the a-Si overlayer of ±8%, results in a PRE penalty of only 1%. These tolerances are all within the process specifications offered by photonic foundries, demonstrating the robustness of our polarization rotator design.

Besides the above geometrical parameters, the thickness of the pad oxide layer between the waveguide core and the a-Si overlayer plays an important role in the rotator efficiency. Horizontal slot waveguide is formed in the pad oxide layer [as shown in Fig. 2(c)], such that the quasi-TM mode is strongly confined in the slot region, resulting in its propagation constant to be highly sensitive to the slot thickness and refractive index. In the simulations presented above, the pad layer material underneath the a-Si overlayer is SiO_2 of thickness $H_{pad} = 10$ nm. The corresponding fabrication tolerance is $\Delta H_{pad} = 2$ nm for PRE > 90%. We find that the fabrication tolerance can be improved by using a pad material with a higher refractive index (e.g., Si_3N_4 with $n_{Si3N4} = 1.989$). If Si_3N_4 is used as a pad spacer, $\Delta H_{Si3N4} = 4$ nm for $H_{Si3N4} = 10$ nm. Therefore, the fabrication tolerance of the Si_3N_4 pad spacer is about twice that of the SiO_2 pad spacer.

Finally, we examine the operating wavelength range of our polarization rotator. By assuming a TE input, the extinction ratio (ER) and the insertion loss (IL) are defined as $ER = 10\log_{10}(P_{TM}^{out}/P_{TE}^{out})$ and $IL = 10\log_{10}(P_{TM}^{out}/P_{TE}^{in})$, respectively. Fig. 7(a) shows the wavelength dependent relative power transmission of the rotator for H = 220 nm assuming a TE polarized input signal. It is observed that ER is > 10 dB for the wavelength range of 1490 nm to 1625 nm (bandwidth > 135 nm), while the calculated ER exceeds 17 dB across the entire C-band (1530 nm to 1565 nm). The calculated

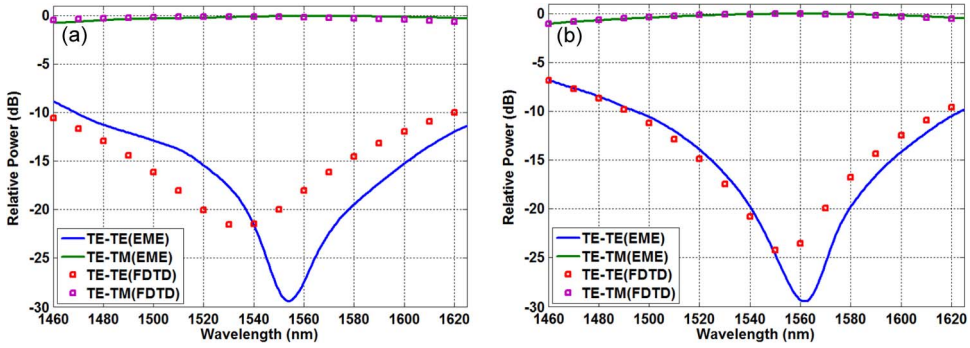

Fig. 7. Wavelength dependence of polarization rotation for TE polarized input calculated by 3D-FDTD and fully vectorial EME simulations. (a) $H = H_R = 220$ nm, $W = 390$ nm, $W_R = 343$ nm and $\theta = 2.4°$; (b) $H = H_R = 260$ nm, $W = 430$ nm, $W_R = 386$ nm and $\theta = 1.7°$.

insertion loss is better than -0.16 dB. The wavelength dependent relative power transmission of the rotator with the 260 nm silicon core for TE input is shown in Fig. 7(b). ER $>$ 10 dB is obtained for the wavelength range of 1500 nm to 1610 nm. This broad bandwidth ($>$ 110 nm) is a distinct advantage of a mode-evolution type polarization rotator. The calculated insertion loss is less than -0.3 dB. The additional insertion loss induced by the sidewall roughness of the composite waveguide is negligible (better than -0.05 dB) by assuming the propagation losses of the c-Si wire waveguide and a-Si wire waveguide to be 3.6 dB/cm [15] and 3.5 dB/cm [16], respectively.

4. Conclusion

We have proposed and demonstrated by simulations a robust polarization rotator design based on the mode-evolution mechanism. The rotator comprises a silicon wire waveguide with an amorphous silicon overlayer and a thin SiO_2 pad layer and it can be fabricated by standard silicon photonics processing without the need for precise lithographic alignments. Our calculations show that a polarization rotation efficiency of $>$ 99% can be readily achieved at the same time as a broadband operation with 90% rotation efficiency within C-band wavelength range. Considering the anticipated device dimensional variations within typical specifications of silicon photonic foundries, the calculated rotation efficiency exceeds 90%.

References

[1] D. Dai, L. Liu, S. Gao, D.-X. Xu, and S. He, "Polarization management for silicon photonic integrated circuits," *Laser Photon. Rev.*, vol. 7, no. 3, pp. 303–328, May 2013.
[2] T. Barwicz, M. R. Watts, M. A. Popovi, P. T. Rakich, L. Socci, F. X. Kärtner, E. P. Ippen, and H. I. Smith, "Polarization-transparent microphotonic devices in the strong confinement limit," *Nature Photon.*, vol. 1, no. 1, pp. 57–60, Jan. 2007.
[3] L. Liu, Y. Ding, K. Yvind, and J. M. Hvam, "Efficient and compact TE-TM polarization converter built on silicon-on-insulator platform with a simple fabrication process," *Opt. Lett.*, vol. 36, no. 7, pp. 1059–1061, Apr. 2011.
[4] Y. Ding, L. Liu, C. Peucheret, and H. Ou, "Fabrication tolerant polarization splitter and rotator based on a tapered directional coupler," *Opt. Express*, vol. 20, no. 18, pp. 20 021–20 027, Aug. 2012.
[5] H. Fukuda, K. Yamada, T. Tsuchizawa, T. Watanabe, H. Shinojima, and S. Itabashi, "Polarization rotator based on silicon wire waveguides," *Opt. Express*, vol. 16, no. 4, pp. 2628–2635, Feb. 2008.
[6] L. Chen, C. R. Doerr, and Y.-K. Chen, "Compact polarization rotator on silicon for polarization-diversified circuits," *Opt. Lett.*, vol. 36, no. 4, pp. 469–471, Feb. 2011.
[7] D. Vermeulen, S. Member, S. Selvaraja, P. Verheyen, P. Absil, W. Bogaerts, D. Van Thourhout, and G. Roelkens, "Silicon-on-Insulator polarization rotator based on a symmetry breaking silicon overlay," *IEEE Photonics Technol. Lett.*, vol. 24, no. 6, pp. 482–484, Mar. 2012.
[8] H. Zhang, S. Das, Y. Huang, C. Li, S. Chen, H. Zhou, M. Yu, P. G.-Q. Lo, and J. T. L. Thong, "Efficient and broadband polarization rotator using horizontal slot waveguide for silicon photonics," *Appl. Phys. Lett.*, vol. 101, no. 2, pp. 021105-1–021105-4, Jul. 2012.
[9] A. V. Velasco, M. L. Calvo, P. Cheben, A. Ortega-Moñux, J. H. Schmid, C. A. Ramos, I. M. Fernandez, J. Lapointe, M. Vachon, S. Janz, and D.-X. Xu, "Ultracompact polarization converter with a dual subwavelength trench built in a silicon-on-insulator waveguide," *Opt. Lett.*, vol. 37, no. 3, pp. 365–367, Feb. 2012.

[10] Z. Wang and D. Dai, "Ultrasmall Si-nanowire-based polarization rotator," *J. Opt. Soc. Amer. B*, vol. 25, no. 5, pp. 747–753, May 2008.
[11] A. Densmore, D. Xu, P. Waldron, S. Janz, P. Cheben, J. Lapointe, A. Delâge, B. Lamontagne, J. H. Schmid, and E. Post, "A silicon-on-insulator photonic wire based evanescent field sensor," *IEEE Photon. Technol. Lett.*, vol. 18, no. 23, pp. 2520–2522, Dec. 2006.
[12] D. X. Xu, A. Densmore, A. Delâge, P. Waldron, R. McKinnon, S. Janz, J. Lapointe, G. Lopinski, T. Mischki, E. Post, P. Cheben, and J. H. Schmid, "Folded cavity SOI microring sensors for high sensitivity and real time measurement of biomolecular binding," *Opt. Express*, vol. 16, no. 19, pp. 15 137–15 148, Sep. 2008.
[13] R. Sun, P. Dong, N. Feng, C. Hong, J. Michel, M. Lipson, and L. Kimerling, "Horizontal single and multiple slot waveguides: optical transmission atlambda = 1550 nm," *Opt. Express*, vol. 15, no. 26, pp. 17 967–17 972, Dec. 2007.
[14] G. Roelkens, D. Van Thourhout, and R. Baets, "High efficiency silicon-on-insulator grating coupler based on a poly-silicon overlay," *Opt. Express*, vol. 14, no. 24, pp. 11 622–11 630, Nov. 2006.
[15] Y. Vlasov and S. McNab, "Losses in single-mode silicon-on-insulator strip waveguides and bends," *Opt. Express*, vol. 12, no. 8, pp. 1622–1631, Apr. 2004.
[16] S. K. Selvaraja, E. Sleeckx, M. Schaekers, W. Bogaerts, D. Van Thourhout, P. Dumon, and R. Baets, "Low-loss amorphous silicon-on-insulator technology for photonic integrated circuitry," *Opt. Commun.*, vol. 282, no. 9, pp. 1767–1770, May 2009.